Radiation Protection Dosimetry (2019), pp. 1–10 doi:10.1093/rpd/ncz292

COVERING THE PATIENT'S ARM SUPPORT IN LEAD REDUCED THE RADIATION DOSE RATE TO THE CARDIOLOGISTS DURING PERCUTANEOUS CORONARY INTERVENTIONS: A PHANTOM STUDY

Atsushi Fukuda[1,2,*] and Pei-Jan Paul Lin[2]
[1]Preparing Section for New Faculty of Medical Science, Fukushima Medical University, 1 Hikarigaoka, Fukushima 960-1295, Japan
[2]Division of Diagnostic Medical Physics, Department of Radiology, Virginia Commonwealth University Medical Center, 1300 East Marshall Street, Richmond, VA 23298-0615, USA

*Corresponding author: ntoki@blue.plala.or.jp

Received 02 September 2019; revised 04 December 2019; editorial decision 05 December 2019; accepted 05 December 2019

The aim of the study was to estimate organ dose rate reduction to a female anthropomorphic phantom, which simulated the cardiologist, during percutaneous coronary interventions (PCI) when the patient's arm support was covered with 0.4-mm lead foil. Organ dose rates were determined using five radiation detectors inserted into the left eye, left thyroid, left breast, left liver lobe and uterus of the phantom. A male anthropomorphic phantom was placed on the examination table of an angiography system. Heart images of the patient phantom were acquired under 10 gantry angulations typical for PCI. The lead-covered arm support did not interfere with any of the cardiac images. The median organ dose rate reductions to the left eye, left thyroid, left breast, left liver lobe and uterus were 7.8, 36.0, 28.8, 35.7 and 33.5%, respectively. The lead-covered arm support substantially reduced scattered radiation to the female cardiologist without interfering with clinical environments.

INTRODUCTION

With the development of new techniques and devices, percutaneous coronary interventions (PCIs) are performed with increasing frequency and are used for the treatment of more complex coronary artery disease[1,2]. It has been reported that the entrance surface air kerma (ESAK) for the patient during PCIs increases with lesion complexity, a previous history of coronary artery bypass grafting, body mass index (BMI), the number of treated lesions and chronic total occlusions[3–5] and that the occupational radiation dose to the cardiologist during PCI increases linearly with the patient's ESAK[6]. Chronic radiation exposure can result in damage to the cardiologist's DNA, increasing as a function of the length of his or her catheterization laboratory experience[7]. In a series of 31 tumor cases involving interventional physicians, Roguin *et al*. observed a disproportionately high prevalence of tumors on the left side of the head and neck; they speculated that this was because the physicians' left side was closer to the primary X-ray beam and scattered radiation during interventions[8].

It is desirable to keep the occupational radiation dose during PCI as low as is reasonably achievable (the 'ALARA' principle)[9]. Accordingly, cardiologists wear lead aprons, thyroid collars and lead glasses. In addition, a lead curtain is hung from the table side rail and the ceiling-suspended lead shield is installed as standard protective devices for cardiovascular angiography systems. However, the patient's arm support, used to facilitate positioning and restrain the arm, is usually made from plastic material and so offers little protection from radiation. In this study, we customized the patient's arm support by covering it with commercially available lead foil tape to help reduce the scattered radiation.

Although the radiation health hazard for the operator of performing PCIs is acknowledged in the cardiology community[10], to the best of our knowledge, there have been no reports of the estimated organ dose rate to the cardiologist during a PCI procedure. The aim of this study was to evaluate by how much the organ dose rate was reduced when using the lead-covered patient's arm support during a PCI procedure as a function of the X-ray tube angle under both fluoroscopic and cine acquisition modes.

MATERIALS AND METHODS

Materials

In this study, we used a dedicated interventional cardiovascular angiography system (Innova 2100; GE Healthcare, Milwaukee, WI) with a 20 × 20 cm flat panel detector. The radiation dose was measured in the clinical and service modes. The system was equipped to calculate and display the dose area

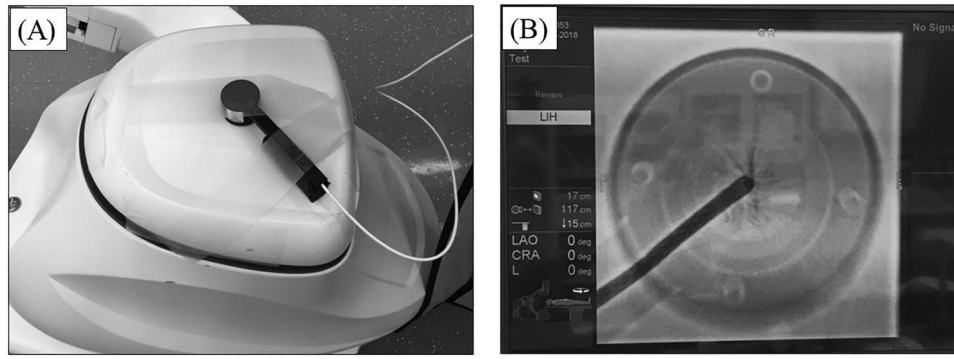

Figure 1. The ionization chamber used to measure the air kerma rate. The 1-cm^3 ionization chamber was attached to the X-ray tube assembly (**A**). The chamber was carefully positioned at the center of the radiation field of view using fluoroscopic imaging (**B**).

product and air kerma (AK) rate at the patient entrance reference point (PERP) when operated in clinical mode[11]. This was not available in the service mode, so a 1-cm^3 ionization chamber (Exradin Magna A600; Standard Imaging, Middleton, WI) was attached to the X-ray tube assembly, carefully positioned in the center of the radiation field of view (FOV), to monitor the radiation output, expressed as the AK rate (Figure 1A and B).

A male anthropomorphic phantom (ATOM Adult Male Model 701; CIRS Inc., Norfolk, VA) was employed to simulate the patient. Its size was based on the International Commission of Radiological Protection (ICRP) 23[12] and the International Commission on Radiation Units and Measurements 48[13]; its height, weight and thorax dimensions were 173 cm, 73 kg and 23 × 32 cm, respectively. A female phantom (ATOM Adult Female Model 702; CIRS Inc., Norfolk, VA) was employed to simulate the cardiologist. This was a cross-sectional dosimetry phantom with 25-mm-thick sections designed for investigations of organ doses. The height, weight and thorax dimensions were 160 cm, 55 kg and 20 × 25 cm, respectively, and it contained predrilled holes (13 mm diameter × 25 mm) for solid-state detectors corresponding to the internal organs or tissue of interests[14]. Dedicated breast attachments (702-BR-350RL; CIRS Inc., Norfolk, VA) were attached bilaterally.

Five solid-state detectors (computed tomography dose profiler, CTDP-2; RTI Electronics, Mölndal, Sweden) calibrated for RQR-5 beam quality were employed to measure the organ doses (Figure 2). These were customized versions of a commercially available CT dose profiler (RTI Electronics, Mölndal, Sweden) with a 1.2-mm^3 (2 × 2 × 0.3 mm) sensor chip, and the sensitive range is from 67 nGy per s to 2.2 Gy per s, with a 10% variation in the energy response between RQR-4 and RQR-10[15].

Figure 2. The CTDP-2 solid-state detector. The solid-state detector employed in this study was customized from a commercially available CTDP.

They were inserted into predrilled holes in the ATOM phantom[16] for the left eye, left thyroid, left breast, left liver lobe and uterus (Figure 3A–E), and the readout signals were provided through customized extended stems. The detectors were connected to a laptop computer through a Barracuda electrometer (RTI Electronics, Mölndal, Sweden) equipped with multiple modules. The five organ doses were simultaneously recorded using Ocean software (RTI Electronics, Mölndal, Sweden).

The patient's arm support was made from four L-shaped acrylic boards (18.0 × 11.8 × 11.8 cm, 3 mm thick). These were connected using commercially available lead foil tape (3M^{TM} Lead Foil Tape 421; 3M Center, St. Paul, MN) with total tape thickness of 0.16 mm, and backing lead thickness of 0.1 mm (Figure 4A and B). The tape was overlapped to achieve a total thickness of at least 0.64 mm, with the lead at least 0.4 mm thick.

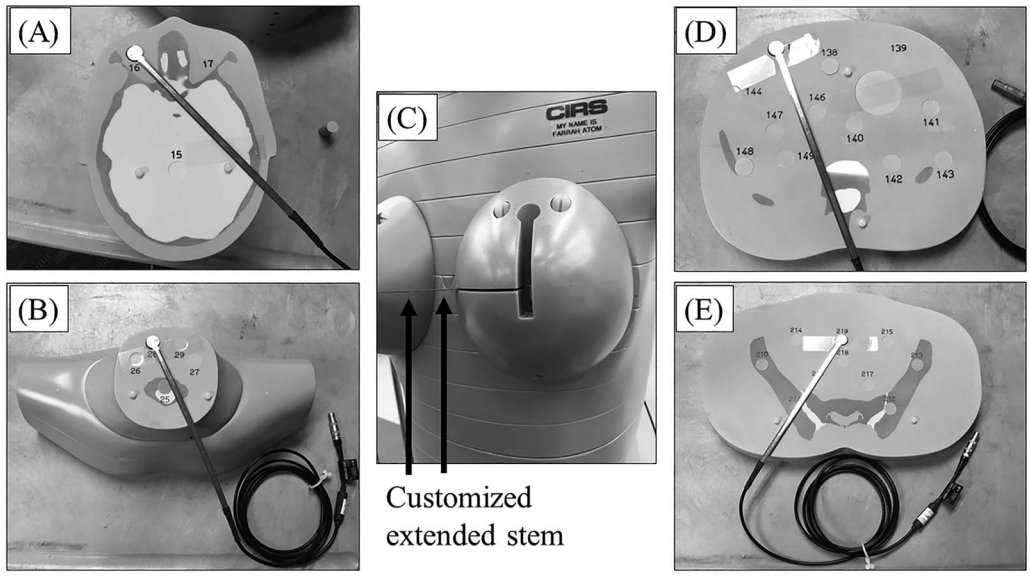

Figure 3. The organ dose rate measurement locations. Organ dose rates were measured at five locations by CTDP-2 solid-state detectors inserted into predrilled holes corresponding to the left eye (**A**), left thyroid (**B**), left breast (**C**), left liver lobe (**D**) and uterus (**E**).

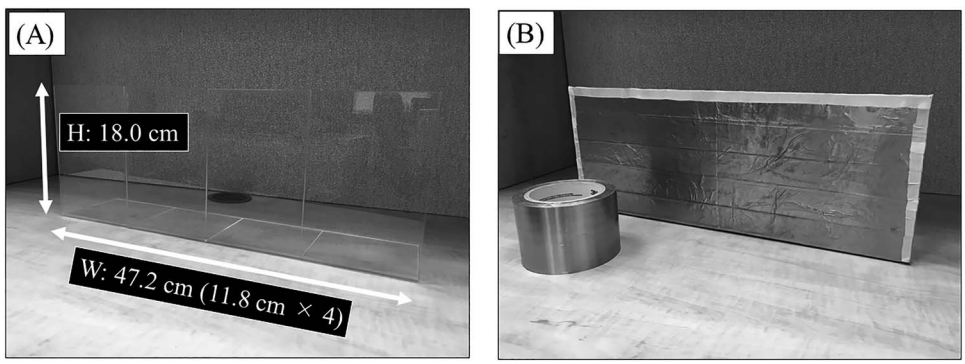

Figure 4. The lead-covered arm support. The four L-shaped acrylic boards were used to make the lead-covered arm support (**A**), connected using commercially available lead foil tape (**B**).

Monitoring the AK rate with an ionization chamber in both clinical and service modes

We measured the organ dose rates to the female cardiologist phantom with the angiography system in service mode (see section of organ dose rate measurement, below). This mode does not offer calculated AK rates at the PERP, so a 1-cm^3 ionization chamber was employed to monitor the AK rate in both clinical and service modes. The ratio of the AK rate can be used to convert between organ dose rates in service mode and those in clinical mode.

Relationship between the automatic parameter setting and X-ray tube angulation

The male patient phantom was set up on the examination table of the cardiovascular angiography system with the heart positioned at the isocenter (Figure 5A and B). For most of the angulation conditions, the tabletop was located 15 cm from the isocenter in the direction of the X-ray tube; however, for the three left anterior oblique (LAO) 45° views, it was moved 5 cm upward to avoid a collision between the examination table and X-ray

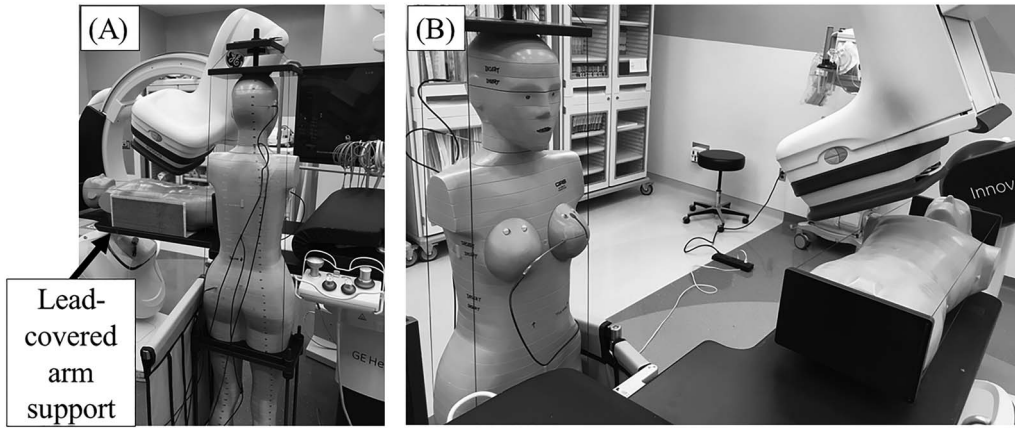

Figure 5. Experimental set up with the two anthropomorphic phantoms and lead-covered arm support. A male anthropomorphic phantom was placed on the examination table to represent the patient, with the lead-covered arm support positioned on the right (arm) side of the phantom (**A**). A female anthropomorphic phantom, representing the cardiologists, was placed adjacent to the right inguinal region of the male phantom (**B**). The left and right images show the RAO 10°/CAU 30° and RAO 30° X-ray tube angulations.

tube assembly. Fluoroscopy and cine acquisitions were carried out at 10 routine X-ray tube angulations in clinical mode (Table 1). The imaging parameters selected for the fluoroscopic and cine acquisition modes were as follows: cardiac and combo, normal (dose) mode, 15 f per s, with a FOV of 17 cm. The following examination parameters were recorded: the source image receptor distance (SID), tube potential, tube current, pulse width, spectral filter, focal spot size, calculated AK rate at the PERP and measured AK rate on the X-ray tube assembly.

Organ dose rate measurement

The female phantom was fixed using 2-cm boards with wires, so the height was 166 cm. After positioning the female phantom adjacent to the right inguinal region of the male phantom (Figure 5A and B), cine acquisitions were carried out in the clinical mode using the same X-ray tube parameters and angulations. However, the scattered radiation level was below that of the detector sensitivity range. To overcome this limitation, the tube current and frame rate were increased to 600 mA and 30 fps, respectively, in the service mode. The organ dose rates and AK rates on the X-ray tube assembly were measured using the same X-ray tube parameters and angulations. Once the data acquisition was complete, the organ dose rates measured using the increased tube current and frame rate were converted to those in clinical mode by multiplying the values by the ratio of the AK rates measured in clinical and service modes.

Statistical analysis

The statistical analyses were performed using R statistical computing software, version 3.5.0. Numerical variables are reported as either mean and standard deviation or median with interquartile range, according to the normality of their distribution. Comparisons of two samples were evaluated using Student's *t*-test, Welch's *t*-test, the paired *t*-test or the exact Wilcoxon rank sum test, according to their distributions. Multiple comparisons of organ dose rates according to the X-ray tube angulation or organ location were evaluated using the Friedman multiple comparison test. *P*-values of 0.05 or less were considered to indicate statistically significant differences.

RESULTS

Relationship between the automatic parameter setting and X-ray tube angulation

Table 1 shows the X-ray parameters pertinent to the fluoroscopy and cine acquisition. The AK rate on the X-ray tube assembly in cine acquisition was 8.8 times higher than that for fluoroscopy ($P < 0.001$). The focal spot sizes for fluoroscopy and cine acquisition were 0.6 and 1.0 mm, respectively, and remained the same for all the x-ray tube angulations. The mean ± standard deviation values for SID in the right anterior oblique (RAO) and LAO views were 105 ± 5 and 102 ± 5 cm, respectively; these were not significant different ($P = 0.51$). The median and interquartile range for the measured AK rate

Table 1. X-ray parameters for the fluoroscopy and cine acquisition.

Geometrical parameters		Fluoroscopy						Cine acquisition					
		X-ray parameters				Radiation output		X-ray parameters				Radiation output	
X-ray tube angulation (°)	SID (cm)	Tube potential (kVp)	Tube current (mA)	Pulse width (ms)	Spectral filter (mmCu)	Calculated AK rate at PERP (mGy per min)	Measured AK rate on X-ray tube assembly (mGy per min)	Tube potential (kVp)	Tube current (mA)	Pulse width (ms)	Spectral filter (mmCu)	Calculated AK rate at PERP (mGy per min)	Measured AK rate on X-ray tube assembly (mGy per min)
0°	92	72.0	12.9	8.7	0.6	8.9 ± 0.1	33.0 ± 0.6	71.9	6.0	5	0.2	77.5 ± 0.3	268 ± 1
RAO 10°/ CAU 30°	108	75.0	11.6	7.4	0.6	9.6 ± 0.1	35.9 ± 0.4	73.0	42.5	5	0.2	91.2 ± 0.9	316 ± 2
RAO 30°/ CAU 30°	108	75.0	15.3	9.8	0.6	15.7 ± 0.1	59.2 ± 0.1	76.8	15.3	5	0.1	164.3 ± 0.6	571 ± 1
RAO 30°	98	73.0	12.5	8.0	0.6	9.1 ± 0.1	33.9 ± 0.5	74.0	33.8	5	0.2	75.7 ± 0.1	267 ± 1
RAO 30°/ CRA 30°	105	82.0	14.4	9.3	0.3	37.3 ± 0.1	148 ± 2	83.0	48.8	6	0	393.3 ± 0.6	1388 ± 5
LAO 10°/ CRA 30°	98	82.0	10.5	6.8	0.3	24.5 ± 0.1	98.1 ± 0.3	81.0	37.2	6	0	280.0 ± 0.1	986 ± 1
LAO 30°/ CRA 30°	98	88.0	11.4	7.8	0.2	43.8 ± 0.1	173.6 ± 0.5	87.0	41.1	7	0	362.3 ± 0.6	1304 ± 2
LAO 45°/ CRA 30°	106	88.0	14.5	9.5	0.2	61.2 ± 0.1	240 ± 6	90.0	52.4	7	0	489.7 ± 0.6	1771 ± 7
LAO 45°	100	82.0	9.6	6.1	0.3	22.1 ± 0.1	88.0 ± 0.3	79.0	36.0	5	0	260.3 ± 0.6	912 ± 1
LAO 45°/ CAU 30°	110	84.0	15.6	10	0.3	46.1 ± 0.1	184.6 ± 0.1	85.0	50.6	7	0	447.3 ± 0.6	1596 ± 3

AK, air-kerma; CAU, caudal; CRA, cranial; LAO, left anterior oblique; PERP, patient entrance reference point; RAO, right anterior oblique; SID, source-image receptor distance.

of the RAO and LAO views in cine acquisition were 444.2 (302.4, 773.8) and 1305 (985.2, 1597) mGy per min; the median AK rate in the LAO view was significantly higher than that in the RAO view ($P < 0.01$).

Organ dose rate measurement

The median organ dose rates to the left eye, left thyroid, left breast, left liver lobe and uterus were 1.25, 1.97, 2.61, 4.49 and 0.56 mGy per h in cine acquisition, respectively (Table 2). The median organ dose rates in LAO views were 4.1–12.5 times higher than those in RAO views ($P < 0.001$). The median left breast and left liver lobe dose rates were 2.1 and 3.6 times higher than the dose rate for the left eye ($P < 0.05$ and $P < 0.001$, respectively). The median left breast and left liver lobe dose rates were 4.6 and 8.0 times higher than the dose rate for the uterus ($P < 0.01$ and $P < 0.001$, respectively). The highest organ dose rates for left eye, left thyroid, left breast, left liver lobe and uterus were 7.68, 11.2, 15.2, 19.8 and 4.05 mGy per h, respectively. These measurements were all obtained with an X-ray tube angulation of LAO 45°/cranial (CRA) 30°. Conversely, the lowest organ dose rates were observed at an X-ray tube angulation of RAO 30° and were significantly different to those obtained at an angulation of LAO 45°/CRA 30° ($P < 0.05$).

The lead-covered arm support was not in the imaging path and so did not interfere with any clinical images. The median reduction (interquartile range) in the dose rate to the left eye with the lead-covered arm support in place was 7.8% (3.3, 39.8%); the median reduction for the LAO views was 5.9 times greater than that for the RAO views ($P < 0.001$). The median reductions in the dose rates to the left thyroid, left breast and left liver lobe with the lead-covered arm support were 36.0 (13.0%, 46.5%), 28.8 (14.8%, 46.9%) and 35.7% (10.7%, 48.7%), respectively. There were no statistically significant differences in these reductions between the RAO and LAO views. The median reduction in the dose rate to the uterus with the lead-covered arm support was 33.5% (13.6%, 51.6%), and the median reduction for the LAO views was 2.7 times higher than that for the RAO views ($P < 0.05$). The most effective angulation with the lead-covered arm support depended on the organ location. For the left eye and the uterus, the most effective angulations were LAO 45° and LAO 45°/CRA 30°, with reductions of 43.3 and 65.2%. For the left thyroid, left breast and left liver lobe, the most effective angulation was RAO 10°/caudal (CAU) 30°, with reductions of 65.5, 76.9, and 63.8%, respectively. Conversely, the lead-covered arm support did not result in reduced organ dose rates at an angulation of RAO 30°/CRA 30°.

DISCUSSION

This study resulted in three main findings. (1) The AK rates for the LAO views were higher than those for RAO views. (2) The organ dose rates were higher with the LAO views than with the RAO views, with the maximum organ dose rates observed at an X-ray tube angulation of LAO 45°/CRA 30°. (3) The lead-covered arm support was effective in reducing the cardiologist's organ dose rates, providing the greatest reductions when the angulation was either RAO 10°/CAU 30° or LAO 45° and LAO 45°/CRA 30°, depending on the organ of interest.

The organ dose rates received by the cardiologist depended on numerous factors. AK rates were higher with the LAO views than with the RAO views, despite there being no statistically significant difference in the SID between these views. During the acquisition of LAO view imaging, the X-rays penetrate along the long axis of the heart, and the higher AK rate is automatically adjusted to obtain an image of diagnostic quality. The increase in AK rate resulted in increased organ dose rates with the LAO views, which were higher than those for the RAO views. However, the tube potentials for the LAO were also higher than those for the RAO views ($P < 0.05$), so the difference could also have been the result of increased scatter from the patient phantom.

The left eye dose rates were lower than the dose rates to the left breast and left liver lobe. This would be expected, because the cardiologist's left eye is usually further than the other organs from the patient's heart and so the dose rate is reduced according to the inverse-square law. With the lead-covered arm support, the reduction in dose rate to the left eye with the RAO views was lower than the reductions for left the breast and left liver lobe. When imaging using the RAO 10° or 30°/CAU 30° views, the flat panel detector assembly is closer to the left eye (Figure 5A) and acts as a radiation protector, reducing dose rate to the left eye. According to ICRP 118, the threshold dose for radiation-induced cataracts is 500 mGy[17]. In this study, the highest left eye dose rate for fluoroscopy was 1.04 mGy per h (calculated as the left eye dose rate in cine acquisition (7.68 mGy per h) × the ratio of measured AK rates for fluoroscopy to cine acquisition (240 mGy per min/1771 mGy per min)), and the highest left eye dose rate for cine acquisition was 7.68 mGy per h; these were at an angulation of LAO 45°/CRA 30° (Tables 1 and 2). These dose rates would reach the threshold level for cataracts in approximately 480 and 65 h, respectively. Haga *et al*. reported that a 75% dose reduction was obtained by wearing 0.07-mm lead glasses[18]. Using both the lead glasses and a lead-covered arm support would yield a dose reduction of 85.6%.

The thyroid gland is one of the most radiosensitive organs, and the effect of thyroid protection can have

Table 2. Organ dose rates to the left eye, left thyroid, left breast, left liver lobe, and uterus in cine acquisition as a function of X-ray tube angulation with and without the lead-covered arm support.

	Left eye				Left thyroid			
	Lead-covered arm support (−)		Lead-covered arm support (+)		Lead-covered arm support (−)		Lead-covered arm support (+)	
X-ray tube angulation (°)	Dose (mGy/h)	PA/RAO/LAO Median dose (mGy/h)	Dose (mG/h)	Reduction (%) (*P*-value)	Dose (mGy/h)	PA/RAO/LAO Median dose (mGy/h)	Dose (mGy/h)	Reduction (%) (*P*-value)
0°	0.61 ± 0.06	0.61	0.59 ± 0.03	3.1 (N.S.)	1.08 ± 0.01	1.08	0.58 ± 0.01	46.7 ($P < 0.001$)
RAO 10°/CAU 30°	0.34 ± 0.05	0.29	0.30 ± 0.02	11.0 (N.S.)	1.06 ± 0.01	0.62	0.37 ± 0.03	65.5 ($P < 0.001$)
RAO 30°/CAU 30°	0.24 ± 0.01		0.23 ± 0.04	3.8 (N.S.)	0.37 ± 0.02		0.28 ± 0.02	25.0 ($P < 0.01$)
RAO 30°	0.25 ± 0.05		0.21 ± 0.03	3.0 (N.S.)	0.27 ± 0.01		0.25 ± 0.01	7.0 (N.S.)
RAO 30°/CRA 30°	0.64 ± 0.03		0.67 ± 0.05	−4.7 (N.S.)	0.88 ± 0.02		0.83 ± 0.02	5.1 (N.S.)
LAO 10°/CRA 30°	1.87 ± 0.11	3.65*	1.78 ± 0.04	4.7 (N.S.)	2.86 ± 0.09	5.94*	2.60 ± 0.03	9.1 ($P < 0.01$)
LAO 30°/CRA 30°	3.53 ± 0.08		2.11 ± 0.02	40.2 ($P < 0.001$)	5.94 ± 0.02		4.22 ± 0.01	29.0 ($P < 0.001$)
LAO 45°/CRA 30°	7.68 ± 0.07		4.41 ± 0.03	42.5 ($P < 0.001$)	11.2 ± 0.1		5.10 ± 0.02	54.4 ($P < 0.001$)
LAO 45°	3.65 ± 0.02		2.07 ± 0.01	43.3 ($P < 0.001$)	5.49 ± 0.03		2.96 ± 0.02	46.1 ($P < 0.001$)
LAO 45°/CAU 30°	6.36 ± 0.05		3.91 ± 0.03	38.5 ($P < 0.001$)	8.75 ± 0.01		4.99 ± 0.03	43.0 ($P < 0.001$)
Median	1.25		1.23	7.8	1.97		1.72	36.0

Continued.

Table 2. Continued.

Left breast				Left liver lobe				Uterus			
Lead-covered arm support (−)		Lead-covered arm support (+)		Lead-covered arm support (−)		Lead-covered arm support (+)		Lead-covered arm support (−)		Lead-covered arm support (+)	
Dose (mGy/h)	PA/RAO/LAO median dose (mGy/h)	Dose (mGy/h)	Reduction (%) (*P*-value)	Dose (mGy/h)	PA/RAO/LAO median dose (mGy/h)	Dose (mGy/h)	Reduction (%) (*P*-value)	Dose (mGy/h)	PA/RAO/LAO median dose (mGy/h)	Dose (mGy/h)	Reduction (%) (*P*-value)
1.21 ± 0.02	1.21	1.04 ± 0.01	14.0 ($P < 0.001$)	1.65 ± 0.05	1.65	1.48 ± 0.03	10.3 ($P < 0.01$)	0.24 ± 0.05	0.24	0.21 ± 0.03	12.5 (N.S.)
1.48 ± 0.03	0.94	0.34 ± 0.05	76.9 ($P < 0.001$)	1.43 ± 0.01	1.58	0.52 ± 0.04	63.8 ($P < 0.001$)	0.52 ± 0.01	0.51	0.40 ± 0.04	22.3 ($P < 0.05$)
0.51 ± 0.04		0.42 ± 0.01	16.9 ($P < 0.05$)	1.73 ± 0.07		1.27 ± 0.04	26.5 ($P < 0.001$)	0.58 ± 0.05		0.48 ± 0.02	16.9 ($P < 0.05$)
0.43 ± 0.03		0.32 ± 0.03	25.0 ($P < 0.05$)	1.24 ± 0.03		1.10 ± 0.03	11.3 ($P < 0.01$)	0.21 ± 0.01		0.10 ± 0.03	50.9 ($P < 0.01$)
1.37 ± 0.01		1.36 ± 0.05	0.9 (N.S.)	4.49 ± 0.04		4.41 ± 0.07	1.9 (N.S.)	0.50 ± 0.03		0.56 ± 0.05	−10.3 (N.S.)
3.73 ± 0.05	8.07*	3.46 ± 0.01	7.3 ($P < 0.05$)	4.48 ± 0.13	9.38*	4.01 ± 0.05	10.5 ($P < 0.01$)	0.54 ± 0.19	2.12*	0.52 ± 0.05	3.4 (N.S.)
8.07 ± 0.04		5.43 ± 0.02	32.7 ($P < 0.001$)	9.38 ± 0.05		5.16 ± 0.03	45.0 ($P < 0.001$)	2.59 ± 0.01		1.43 ± 0.01	44.8 ($P < 0.001$)
15.2 ± 0.1		6.80 ± 0.03	55.1 ($P < 0.001$)	19.8 ± 0.1		9.25 ± 0.02	53.3 ($P < 0.001$)	4.05 ± 0.09		1.41 ± 0.08	65.2 ($P < 0.001$)
7.23 ± 0.03		3.74 ± 0.04	48.2 ($P < 0.001$)	8.44 ± 0.05		4.24 ± 0.05	49.7 ($P < 0.001$)	1.56 ± 0.03		0.59 ± 0.03	62.3 ($P < 0.001$)
11.0 ± 0.1		6.27 ± 0.02	42.9 ($P < 0.001$)	12.0 ± 0.1		6.57 ± 0.01	45.4 ($P < 0.001$)	2.12 ± 0.06		1.02 ± 0.04	51.8 ($P < 0.001$)
2.61**,†		2.41	28.8	4.49***,‡		4.13	35.7	0.56		0.54	33.5

Data are presented as means and standard deviations.

Differences were evaluated for statistically significant differences by Student's *t*-test or Welch's *t*-test for differences between the organ dose rates with and without lead-covered arm support, by the exact Wilcoxon rank sum test for differences between the median organ dose rates in the right and left anterior oblique (RAO and LAO, respectively) views and by the Friedman multiple comparison test for differences among the median organ dose rates to left eye, left thyroid, left breast, left liver lobe and uterus.

N.S., not significant; N.A., not applicable.

*The median organ dose rates in LAO views were 4.1–12.5 times higher than those in RAO views ($P < 0.001$).

**The median left breast dose rate was 2.1 times higher than the left eye dose rate ($P < 0.05$).

***The median left liver lobe dose rate was 3.6 times higher than the left eye dose rate ($P < 0.001$).

†The median left breast dose rate was 4.6 times higher than the uterus dose rate ($P < 0.01$).

‡The median left liver lobe dose rate was 8.0 times higher than the uterus dose rate ($P < 0.001$).

a considerable influence on the magnitude of the effective dose[19]. In addition to the radiation-related thyroid cancer[20], it has recently been reported that benign structural and functional thyroid disease can develop as a result of radiation exposure[21]. As yet, there is insufficient evidence to establish a definite radiation threshold for the benign structural and functional thyroid disease; nevertheless, it is important to comply with the ALARA concept. In the present study, the highest left thyroid dose rates for fluoroscopy and cine acquisition were 1.52 and 11.2 mGy per h with LAO 45°/CRA 30°; the use of the lead-covered arm support reduced these doses by 54.4%. von Boetticher *et al*. reported that the use of an additional thyroid protection collar reduced the dose to the thyroid by 70%[19]; using both a thyroid collar and the lead-covered arm support would therefore yield a reduction in dose of 86.3%.

According to ICRP 103, the tissue weighting factor for the breast should now be 0.12[22]. Previously, the weighting factor used was 0.05; this change results in a noticeable increase in the effective dose to cardiologist. Conversely, ICRP reduced the tissue weighting factor for the liver from 0.05 to 0.04 and for the uterus (gonads) from 0.20 to 0.08. These changes resulted in small decreases in the effective dose to the cardiologist; however, the liver and uterus (gonads) are considered to be radiosensitive organs, and appropriate radiation shielding is recommended. Cardiologists use lead aprons 0.25, 0.35 or 0.50 mm thick, which reduce the amount of scattered radiation by 89, 94 and 97%, respectively[19]. Wearing a 0.35-mm lead apron in conjunction with the use of the lead-covered arm support could reduce the organ doses for the left breast, left liver lobe and uterus with LAO 45°/CRA 30° by over 97.2%.

According to the ICRP, when a female cardiologist declares she is pregnant, the equivalent dose to fetus should be kept under 1 mSv during the remainder of her pregnancy. In the present study, the highest uterus dose rates with fluoroscopy and cine acquisition were 0.55 and 4.05 mGy per h, respectively, with the LAO 45°/CRA 30° angulation. These values can be converted to equivalent doses to the uterus by using the ratio of the mass energy absorption coefficients for the uterus (ovary) and air[23]; this results in converted equivalent dose rates to the uterus with fluoroscopy and cine acquisition of approximately 0.58 and 4.3 mSv per h, respectively. Wearing a 0.35-mm lead apron in conjunction with the use of lead-covered arm support, the equivalent doses to the uterus reach the dose limit in approximately 82 hours for fluoroscopy and 11 hours for cine acquisition.

This study had some limitations. All the organ dose rates were measured without the lead apron and the ceiling-suspended lead shield which are routinely used by the cardiologists in most PCI because the scattered radiation level was below that of the detector sensitivity range. However, with the lead apron and the ceiling-suspended lead shield, the transmitted radiation has a different quality: as a consequence, it is expected that the dose reduction factors of the lead-covered arm support would be partially different from the ones measured without the lead apron and the ceiling-suspended lead shield.

The results demonstrated that the lead-covered arm support reduced the organ dose rates during 10 routine X-ray angulations; however, a lateral (90°) view may be required during PCI. If the primary beam penetrates the lead-covered arm support, automatic exposure control will vary and increase the AK rate to compensate for the flat panel detector input dose, which would result in unnecessary radiation exposure to the patient; thus, the lead-covered arm support should be removed before imaging with a lateral view.

The dose reductions with the lead-covered arm support were established on the assumption that the PCI used bilateral femoral access. Radial access is also used for PCI; however, the lead-covered arm support would not be employed in this geometry, so alternative protection would be essential[24].

We employed two anthropomorphic male and female phantoms. A higher AK rate would be necessary for patients with higher BMI, with the organ dose rate to the cardiologist increasing as a function of the AK rate. The female phantom was designed to have the physique of an internationally averaged woman; a different height and weight would affect the organ dose rates.

CONCLUSIONS

In this study, we measured the AK rate of the X-ray tube assembly and estimated the organ dose rates to the cardiologist's left eye, left thyroid, left breast, left liver lobe and uterus for 10 typical routine gantry angulations. The AK rate and all organ dose rates measured with the LAO views were higher than those with the RAO views. For the left eye and the uterus, using the lead-covered arm support reduced the organ dose rates with the LAO 45° and LAO 45°/CRA 30° views by 43.3 and 65.2%, respectively. For the left thyroid, left breast and left liver lobe, using the lead-covered arm support with the RAO 10°/CAU 30° view reduced the organ doses by 65.5, 76.9, and 63.8%, respectively. It is therefore recommended that a lead-covered arm support is used whenever possible during PCI procedures in line with the ALARA concept.

FUNDING

None.

REFERENCES

1. Dehmer, G. J. *et al. A contemporary view of diagnostic cardiac catheterization and percutaneous coronary intervention in the United States: a report from the CathPCI Registry of the National Cardiovascular Data Registry, 2010 through June 2011*. J. Am. Coll. Cardiol **60**(20), 2017–2031 (2012). doi: 10.1016/j.jacc.2012.08.966.
2. Prasad, A., Rihal, C. S., Lennon, R. J., Wiste, H. J., Singh, M. and Holmes, D. R. J. *Trends in outcomes after percutaneous coronary intervention for chronic total occlusions: a 25-year experience from the Mayo Clinic*. J. Am. Coll. Cardiol. **49**(15), 1611–1618 (2007). doi: 10.1016/j.jacc.2006.12.040.
3. Suzuki, S., Furui, S., Kohtake, H., Yokoyama, N., Kozuma, K., Yamamoto, Y. and Isshiki, T. *Radiation exposure to patient's skin during percutaneous coronary intervention for various lesions, including chronic total occlusion*. Circ. J. **70**(1), 44–48 (2006).
4. Fetterly, K. A., Lennon, R. J., Bell, M. R., Holmes, D. R. J. and Rihal, C. S. *Clinical determinants of radiation dose in percutaneous coronary interventional procedures: influence of patient size, procedure complexity, and performing physician*. JACC. Cardiovasc. Interv **4**(3), 336–343 (2011). doi: 10.1016/j.jcin.2010.10.014.
5. Delewi, R. *et al. Clinical and procedural characteristics associated with higher radiation exposure during percutaneous coronary interventions and coronary angiography*. Circ. Cardiovasc. Interv. **6**(5), 501–506 (2013). doi: 10.1161/CIRCINTERVENTIONS.113.000220.
6. Vano, E., Ubeda, C., Leyton, F., Miranda, P. and Gonzalez, L. *Staff radiation doses in interventional cardiology: correlation with patient exposure*. Pediatr. Cardiol. **30**(4), 409–413 (2009). doi: 10.1007/s00246-008-9375-0.
7. Andreassi, M. G., Cioppa, A., Botto, N., Joksic, G., Manfredi, S., Federici, C., Ostojic, M., Rubino, P. and Picano, E. *Somatic DNA damage in interventional cardiologists: a case-control study*. **19**(8), 998–FASEB. J, 999 (2005).
8. Roguin, A., Goldstein, J., Bar, O. and Goldstein, J. A. *Brain and neck tumors among physicians performing interventional procedures*. Am. J. Cardiol. **111**(9), 1368–1372 (2013). doi: 10.1016/j.amjcard.2012.12.060.
9. Cousins, C. *et al. International Commission on Radiological Protection. ICRP publication 120: Radiological protection in cardiology*. **42**(1), 1–Ann. ICRP, 125 (2013). doi: 10.1016/j.icrp.2012.09.001.
10. Pavlidis, A. N., Jones, D. A., Sirker, A., Mathur, A. and Smith, E. J. *Reducing radiation in chronic total occlusion percutaneous coronary interventions*. Curr. Cardiol. Rev. **12**(1), 12–17 (2016).
11. International Electrotechnical Commission. Medical Electrical Equipment: Part 2-43 Particular Requirements for the Basic Safety and Essential Performance of X Ray Equipment for Interventional Procedures (IEC 60601-2-43), second edn. (Geneva, Switzerland: IEC) (2010).
12. International Commission on Radiological Protection. Report of the Task Group on Reference Man. Vol. **23**. (Oxford, UK: ICRP Publication) (1975).
13. International Commission on Radiation Units and Measurements. *Phantoms and computational models in therapy, diagnosis and protection. ICRU Report 48*. J. ICRU. **25**(1) (1992).
14. Computerized Imaging Reference Systems (CIRS). User Guide of Adult Female Phantom (Model 702). (Virginia, USA: CIRS) (2010).
15. RTI Electronics. CT Dose Profiler User's Manual. (Mölndal, Sweden: RTI) (2014).
16. Matsubara, K., Lin, P. J., Fukuda, A. and Koshida, K. *Differences in behavior of tube current modulation techniques for thoracic CT examinations between male and female anthropomorphic phantoms*. Radiol. Phys. Technol **7**(2), 316–328 (2014). doi: 10.1007/s12194-014-0269-y.
17. International Commission on Radiological Protection. *ICRP publication 118: ICRP statement on tissue reactions and early and late effects of radiation in normal tissues and organs–threshold doses for tissue reactions in a radiation protection context*. Ann. ICRP **41**(1–2), 1–322 (2012). doi: 10.1016/j.icrp.2012.02.001.
18. Haga, Y., Chida, K., Kaga, Y., Sota, M., Meguro, T. and Zuguchi, M. *Occupational eye dose in interventional cardiology procedures*, *569*. Sci. Rep **7**(1) (2017). doi: 10.1038/s41598-017-00556-3.
19. von Boetticher, H., Lachmund, J. and Hoffmann, W. *Cardiac catheterization: impact of face and neck shielding on new estimates of effective dose*. Health. Phys **97**(6), 622–627 (2009). doi: 10.1097/01.HP.0000363843.01041.99.
20. National Council on Radiation Protection and Measurements. Risk to the thyroid from ionizing radiation NCRU Report No. 159 (2008).
21. Ron, E. and Brenner, A. *Non-malignant thyroid diseases after a wide range of radiation exposures*. Radiat. Res. **174**(6), 877–888 (2010). doi: 10.1667/RR1953.1.
22. International Commission on Radiological Protection. *The 2007 recommendations of the international commission on radiological protection. ICRP publication 103*. Ann. ICRP **37**(2-4), 1–332 (2007).
23. International Commission on Radiation Units and Measurements. ICRU report 44: tissue substitutes in radiation dosimetry and measurement. (ICRU) (1989).
24. Kallinikou, Z., Puricel, S. G., Ryckx, N., Togni, M., Baeriswyl, G., Stauffer, J. C., Cook, S., Verdun, F. R. and Goy, J. J. *Radiation exposure of the operator during coronary interventions (from the RADIO Study)*. Am. J. Cardiol. **118**(2), 188–194 (2016). doi: 10.1016/j.amjcard.2016.04.045.